Anal. Chem. **1999,** *71,* 939−946

Articles

Trace Element Microanalysis in Iron Meteorites by Laser Ablation ICPMS

Andrew J. Campbell* and Munir Humayun

Department of the Geophysical Sciences, The University of Chicago, Chicago, Illinois 60637

A laser ablation microanalysis system has been developed that can analyze trace elements with a sensitivity in the ppb range, using a CETAC LSX-200 laser ablation system with a Finnigan Element. This capability has been applied to a set of iron meteorites to demonstrate the laser microprobe's analytical capability for the determination of platinum group elements (PGEs) with a spatial resolution of ~20 μm, comparable to that of dynamic secondary ion mass spectrometry (SIMS). The laser is shown to provide an accurate means of solid sampling for magnetic sector inductively coupled plasma mass spectrometry (ICPMS), allowing the determination of bulk metal composition, chemical zoning within the sample, and depth profiling. Recovery of the chemical zoning in taenite lamellae was achieved for Ru, Rh, and Pd, which was not previously possible using SIMS. The methods presented here show that magnetic sector ICPMS can be successfully coupled to a laser ablation system, providing the advantages of higher sensitivity of the sector instrument, low background count rates (<0.1 counts/s), and flat-topped spectral peaks, while minimizing tradeoff against the speed of data acquisition required to handle the transient signals from the laser ablation system.

The study of trace element distribution in metals finds applications in cosmochemistry (Fe−Ni alloys in meteorites), experimental geochemistry (metal−silicate equilibria), economic geology (native metals), metallurgy (steels, etc.), and archeology (metal artifacts). Critical to our understanding of the origin of natural and ancient metals is a detailed knowledge of the composition of these substances, particularly at spatial scales on the order of micrometers.[1] Most metals are alloys, the physical and chemical properties of which depend significantly on the presence of exsolution lamellae, that represent grains of a low-temperature phase that have exsolved from a high-temperature host. Cooling histories of metals can be derived from measured diffusion profiles across the exsolution lamellae, and these are essential in the study of natural and ancient metals for which no other records are available.

One important class of elements in ferrous metals is the platinum group elements (PGEs) (including Ru, Rh, Pd, Os, Ir, and Pt) and those closely related in chemical properties, Re and Au. These are rare elements (few hundreds of ppb in cosmic material, lower in others), which partition preferentially into Fe−Ni alloys in molten silicate and sulfide systems.[2] Another important property is the condensation temperature of these elements, which ranges from the most refractory materials in the solar nebula (metal nuggets of Re, Os, Ru, and Ir alloys) to volatile Au, with intermediate values for the major element Fe (and associated Co and Ni). Thus, studies of these elements in fremdlinge (PGE-rich metal−sulfide assemblages) from carbonaceous chondrites provide information on their condensation sequence from the solar nebula.[3]

These elements also partition between solid Fe and liquid Fe−Ni−S melt such that Re, Os, and Ir are greatly concentrated in the solid, Ru and Pt partition less strongly into the solid, and Au and Pd enter the liquid; hence PGE compositions provide information on the crystallization of molten metal that forms iron meteorites. Elemental analysis provides the basic means of classifying iron meteorites and assigning these to distinct parent bodies.[4] Such analysis has revealed that iron meteorites fall into 13 major groups, with many more ungrouped irons, and probably as many parent bodies represented. This is significantly more than those known from the study of complimentary silicate objects (about five differentiated parent bodies), which is generally ascribed to the superior resistance of irons against collision-induced fragmentation. Besides classification, PGE analyses also provide genetic information on the composition of parental materials, their extent of oxidation, the degree of melting of the parent body, and the degree of fractional crystallization occurring.[5,6] These chemical analyses have been largely carried out by neutron activation analysis (NAA), which remains the principal method for iron meteorite analysis.

* Corresponding author: (e-mail) acampbel@midway.uchicago.edu; (phone) (773) 834-1523; (fax) (773) 702-9505.

(1) Hsu, W.; Huss, G. R.; Wasserburg, G. J. *Lunar Planet. Sci. Conf.* **1998**, *29*, 1781.

(2) Righter, K.; Drake, M. J.; Yaxley, G. *Phys. Earth Planet. Int.* **1997**, *100*, 115. Jones, J. H.; Malvin, D. J. *Metall. Trans. B* **1990**, *21B*, 697.

(3) Sylvester, P. J.; Simon, S. B.; Grossman, L. *Geochim. Cosmochim. Acta* **1993**, *57*, 3763. Sylvester, P. J.; Ward, B. J.; Grossman, L.; Hutcheon, I. D. *Geochim. Cosmochim. Acta* **1990**, *54*, 3491. Palme, H.; Hutcheon, I. D.; Spettel, B. *Geochim. Cosmochim. Acta* **1994**, *58*, 495.

(4) Scott, E. R. D. *Geochim. Cosmochim. Acta* **1972**, *36*, 1205. Wasson, J. T. *Meteorites*; Freeman: New York, 1995.

(5) Davis, A. M., Ph.D. Thesis, Yale University, 1977.

(6) Kelly, W. R.; Larimer, J. W. *Geochim. Cosmochim. Acta* **1977**, *41*, 93.

10.1021/ac9808425 CCC: $18.00
Published on Web 01/21/1999

Direct radiometric ages of initial crystallization and subsequent cooling have been obtained on iron meteorites using the decay of short-lived ^{107}Pd (to ^{107}Ag, $\lambda = 1.07 \times 10^{-7}$ yr^{-1}) and long-lived ^{187}Re (to ^{187}Os, $\lambda = 1.666 \times 10^{-10}$ yr^{-1}) and ^{190}Pt (to ^{186}Os, $\lambda = 1.542 \times 10^{-12}$ yr^{-1}) radioisotopes.[7,8] A knowledge of the internal microdistribution of Pd, Ag, Re, Os, Pt, and related elements is crucial to selecting appropriate samples for geochronological studies of the iron meteorites, since these reveal subtle metamorphic and shock heating-induced redistribution of parent and daughter nuclides.

This report will focus on the microanalysis of PGEs, Re and Au in Fe−Ni alloys occurring naturally as iron meteorites, since these constitute a group of materials for which the chemical abundances of many trace elements are reasonably well-known by NAA. During cooling of meteorite parent bodies, the high-temperature Fe−Ni alloy (γ-Fe) undergoes a subsolidus phase transition to a two-phase mixture of kamacite (α-Fe, Ni-poor) and taenite (γ-Fe, Ni-rich). Diffusional profiles determined by electron microprobe analysis of Ni in the taenite allow calculation of the cooling histories of the meteorites, which are important constraints on the size of meteorite parent bodies. Detection limits of these widely used techniques (100 ppm) have impeded the recovery of corresponding information on trace elements.

In the present work, both the bulk chemical composition and the internal chemical zoning within iron meteorites are measured, using laser ablation as a solid sampling tool with magnetic sector, high-resolution inductively coupled plasma mass spectrometry (HR-ICPMS). Compared to other microanalytical techniques,[1] the use of laser ablation ICPMS can greatly extend both the number of elements and the abundance range over which these elements can be measured. The technique can be further extended to other elements in iron meteorites, to determination of trace elements in metals in other types of meteorites, and to the analysis of metal matrixes in general.

Most of the previous development work on the laser ablation ICPMS technique has relied on quadropole mass spectrometers.[9,10] A wide variety of sample materials has been studied, including one previous application to iron meteorites.[11] In the present study, laser ablation solid sampling is coupled to a high-resolution, magnetic sector ICPMS, which provides better sensitivity with lower background (<0.1 counts/s). This paper describes the laser coupling with metal which is critical to the ablation sampling process, the signal brightness and reproducibility, and the calibration of the signal to yield concentrations. Strategies are also outlined for recovering chemical information in inhomogeneous samples that form the basis for the use of this technique as a microprobe. Examples applied to iron meteorites are provided as validation of the method of laser ablation using magnetic sector ICPMS.

EXPERIMENTAL SECTION

A commercial laser ablation system (LSX-200, CETAC Technologies Inc.) was coupled to a magnetic sector ICPMS (Element, Finnigan MAT) to further develop laser ablation as a microanalytical peripheral for use with magnetic sector ICPMS. These systems, and the specific analytical protocols required to produce reliable data, are detailed below. The laser ablation peripheral is normally operated in one of several data collection modes. Following the description of the apparatus, the advantages and drawbacks of point analysis mode, line scan mode, and depth profiling will each be considered in turn.

Mass Spectrometer. The Element is a magnetic sector, single collector ICP mass spectrometer, with a reverse Nier−Johnson geometry (magnetic sector followed by electric sector). The mass resolution of the instrument is set by three fixed slit settings that offer low ($R = 340$), medium ($R = 4300$), and high ($R = 9300$) resolution, capable of resolving nearly all molecular isobaric interferences on atomic ions. For most data collection, we operate the Element in low-resolution ($R = 340$) mode, with flat-topped peaks, and a sensitivity of 1 million counts s^{-1} ppb^{-1} at ^{115}In for nebulized solution. The instrument can be operated in high-resolution mode to determine which isotopes are free of interferences to use for measuring abundances. Above $R = 340$, there is a loss of sensitivity by a factor of 10−50 and peaks are no longer flat-topped. A mass spectrum featuring a scan over 150% of each peak width is shown in Figure 1.

Each analysis is composed of multiple sweeps across the entire mass range of interest. Within each sweep the mass spectrometer is programmed to "hop" between peaks and then scan across each peak while recording the signal. Peaks can be scanned at a user-selected percentage of the mass range; in low resolution, 10% of the flat-topped portion of the peak is scanned before hopping to the next peak. Magnetic sector ICP instruments scan more slowly than quadrupole-based instruments, as the result of hysteresis in the electromagnet, requiring longer settling times. The laminated magnet of the Element is capable of hopping across the mass spectrum from 6 to 260 amu in under 300 ms, with a settling time of 1 ms/amu; alternatively, a rapid electric scan allows hopping 20% of a fixed magnet mass in 1 ms. For each experiment, a suitable compromise must be met between scanning the peaks slowly to maximize the time-on-peak of each sweep, and scanning rapidly to negate the effects of the time-dependence of some laser ablation signals, described below.

The detector is a dual-mode, 20-stage secondary electron multiplier that can be operated in either analog mode (10^3−10^8 counts/s) or in ion counting mode (10^{-2}−10^6 counts/s), with a dark noise of 0.02−0.08 counts/s. Element software allows a calibration between the two modes to be performed using any signal less than 10^6 counts/s; this calibration is precise to <1.5% using the convenient 10^4 counts/s ^{84}Kr background signal from Ar gas impurity. Because of the curved flight path and narrow slits of the Element, no light blocking is needed and no photons reach the detector. The effective detection limit imposed by

(7) Kelly, W. R.; Wasserburg, G. J. *Geophys. Res. Lett.* **1978**, *5*, 1079. Chen, J. H.; Wasserburg, G. J. *Geochim. Cosmochim. Acta* **1990**, *54*, 1729. Smoliar, M. I.; Walker, R. J.; Morgan, J. W. *Science* **1996**, *271*, 1099. Walker, R. J.; Morgan, J. W.; Beary, E. S.; Smoliar, M. I.; Czamanske, G. K.; Horan, M. F. *Geochim. Cosmochim. Acta* **1997**, *61*, 4799.

(8) Shen, J. J.; Papanastassiou, D. A.; Wasserburg, G. J. *Geochim. Cosmochim. Acta* **1996**, *60*, 2887.

(9) Arrowsmith, P. *Anal. Chem.* **1987**, *59*, 1437. Cromwell, E. F.; Arrowsmith, P. *Anal. Chem.* **1995**, *67*, 131. Morrison, C. A.; Lambert, D. D.; Morrison, R. J. S.; Ahlers, W. W.; Nicholls, I. A. *Chem. Geol.* **1995**, *119*, 13. Shepherd, T. J.; Chenery, S. R. *Geochim. Cosmochim. Acta* **1995**, *59*, 3997. Bea, F.; Montero, P.; Stroh, A.; Baasner, J. *Chem. Geol.* **1996**, *133*, 145. Machado, N.; Gauthier, G. *Geochim. Cosmochim. Acta* **1996**, *60*, 5063. Audetat, A.; Gunther, D.; Heinrich, C. A. *Science* **1998**, *279*, 2091. Eggins, S. M.; Rudnick, R. L.; McDonough, W. F. *Earth Planet. Sci. Lett.* **1998**, *154*, 53.

(10) Norman, M. D.; Pearson, N. J.; Sharma, A.; Griffin, W. L. *Geostand. Newslett.* **1996**, *20*, 247.

(11) Hirata, T.; Nesbitt, R. W. *Earth Planet. Sci. Lett.* **1997**, *147*, 11.

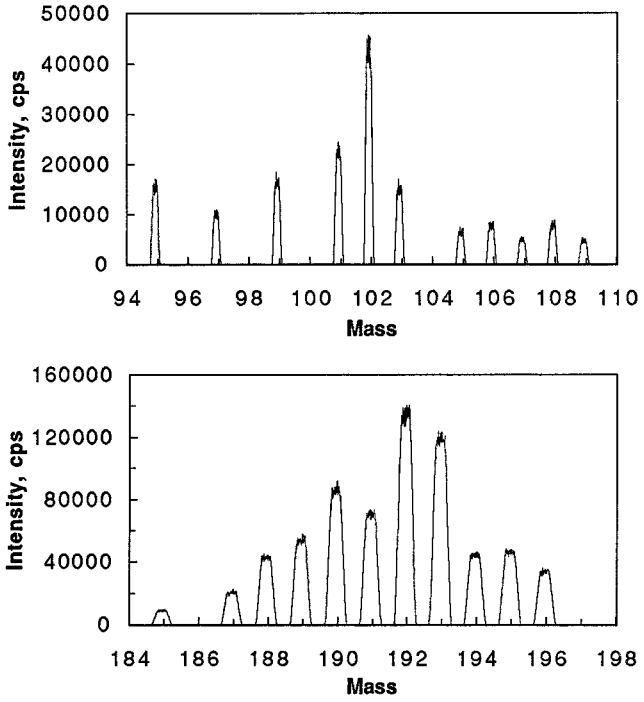

Figure 1. Mass spectrum of Mo−Ag and Re−Au obtained on Hoba (IVB) by laser ablation. This figure is to illustrate signal quality; in normal data collection, only the central 10% of the peak is scanned. All of the data shown were recorded in the same experiment; the figure is set into two panes for clarity.

instrumental considerations is less than 1 fg/g using solution nebulization techniques. The practical detection limit is then imposed by memory effects in the sampling and source systems. Successful analyses of PGE solutions with blank levels of <10 fg/g have been performed with this system.

Laser Ablation. A LSX-200 UV laser ablation microprobe was recently installed on the Element to facilitate in situ microanalysis. The laser is a frequency-quadrupled Nd:YAG laser operating at 266 nm, with <6-ns pulse duration, 1−20-Hz variable repetition rate, and capable of delivering a maximum pulse energy of 3.3 mJ to the sample. The laser energy, repetition rate, and number of pulses are user selected. The pulse energy can be controlled with both the energy level of the laser and a motorized, polarizing attenuator. The diameter of the ablated pit is dependent on the energy level of the laser and the setting of the adjustable beam expander and can be reduced to under 20 μm in diameter. The sample is perched on a software-controlled, motorized stage (1.25 μm stepped movement), and viewed with a binocular microscope and by a CCD camera, the image of which is displayed on a Sony Trinitron monitor. Zoom capability allows magnification from 80 to 800×.

Samples fitting the 2-in.-diameter chamber of the LSX-200 can be conveniently accommodated. Flat, unpolished surfaces are often preferable to polished surfaces, to prevent reflection or transmission of laser light. The sample can be viewed in transmitted or reflected light with a binocular microscope or by its CCD camera image. Aerosol is transported to the torch via Tygon tubing, with an uptake time of a few seconds. The washout time following the end of ablation is 5 s per order of magnitude that the signal drops. A spray chamber significantly improves stability; however, signal intensity drops because of aerosol loss in the spray chamber, and uptake/washout times are lengthened considerably. The analyses discussed below were carried out without the use of a spray chamber.

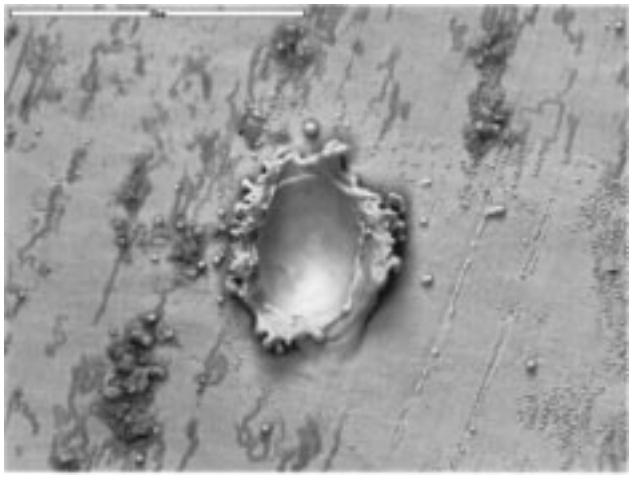

Figure 2. SEM image of a laser-ablated spot on Fe foil. Note the ejected melt blobs lying outside the region of ablation. Scale bar, 50 μm.

The use of an ultraviolet laser source, instead of an infrared beam, allows both a smaller ablated spot diameter to be achieved with any given optical arrangement and enhanced coupling of the laser light to the sample, particularly in the case of nonmetallic specimens.[12] The laser ablation process with metal targets is largely that of melting and vaporization, because the time scale for dissipating the absorbed energy (~ps) is short compared to the laser pulse length (~ns).[13] This is illustrated in an SEM image of a laser-ablated spot on an iron foil (Figure 2), where smooth surface features related to melting are obvious. Note also the presence of melt ejecta in Figure 2; the largest particles leaving the ablated spot settle nearby on the sample surface. This is particularly evident in line-scanning mode, where the ablated volumes are typically larger (discussed below). Smaller particles are also expected to condense from the plasma that forms above the sample surface during laser ablation.[13] The interaction of a laser pulse with a silicate is more complicated than with a metal because of a wider range of electronic excitations available to the insulator.[13] Thermal effects from laser ablation of silicates are still detectable but not as obvious as in Figure 2.

The volume of material ablated depends not only on the characteristics of the laser pulse but also on the optical, electronic, and thermodynamic properties of the sample and the surface characteristics of the target specimen. Of key importance, for example, is the melting point of the sample. By estimating the volume of ablated pits in metals using optical microscopy, it was determined that the ablation rate for Al (melting point 660 °C) was ~20 times greater than that of W (melting point 3410 °C), with metals having intermediate melting points (Ta, Mo, Zr) having appropriately intermediate ablation rates. It is evident that more refractory metals require higher energies than volatile metals for a unit volume of material to be ablated from the sample.

(12) Sylvester, P. J.; Ghaderi, M. *Chem. Geol.* **1997**, *141*, 49.
(13) von Allmen, M.; Blatter, A. *Laser-Beam Interactions with Materials*, 2nd ed.; Springer: Berlin, 1995. Miller, J. C. *Laser Ablation*; Springer-Verlag: Berlin, 1994.

Nonmetals are not expected to follow the same scaling between laser power and ablated volume, because the mechanisms of laser absorption are different from that of the metals studied.

The ion yield of the instrument, that is, the number of ions detected per atoms ablated, can be calculated from the ablation rates and the measured count rate at a given isotope. For ^{193}Ir in the iron meteorite Hoba, the ablation rate at 3.3 mJ pulse energy is 6400 μm^3 per shot and the measured count rate for a train of such pulses is 2.0×10^6 counts/s; from this and the concentration of 23 ppm Ir in Hoba, an ion yield of 4.4×10^{-5} is determined. This result is sensitive to the pulse energy and spot diameter, but most sensitive to the ionic mass and first ionization potential (FIP), with heavier ions and lower FIPs providing higher yields. For comparison, the ion yield of ^{139}La from the NIST 612 silicate glass standard under identical conditions was measured as 3.1×10^{-5}, with an ablation rate 2−3 times that of Hoba. The difference in these ion yields can be largely attributed to the difference in mass and FIP between La and Ir, although other factors such as the ablated particle size distribution may also have an effect. Comparable ion yields for solution nebulization methods using the Element are $\sim 10^{-3}$ with a CETAC MCN 6000 nebulizer.

A mass spectrum of the PGEs in an iron meteorite, Hoba IVB, produced by laser ablation, shown in Figure 1, illustrates the flat-topped peak profiles from the Element mass spectrometer as well as the high intensities of the laser ablation signal. The Ag peaks are from ubiquitous contaminants, as reflected by both the high abundance and normal isotopic ratio of ^{107}Ag/^{109}Ag, which are grossly different from those reported[14] for this meteorite.

Calibration. Several different methods of standardization can be utilized. External standard methods, where concentrations are calculated relative to the intensity measured from a known standard, can in principle be used. However, because of the known large dependence of the signal intensity on material properties such as the melting point (i.e., a large matrix effect), it is critical that the standard be very similar to the sample. It is therefore preferable that internal standardization be used. In this approach, the concentration of at least one major or minor element is independently known, and intensity ratios obtained relative to this element are used for calibration. For greatest accuracy, a set of instrumental sensitivity factors is determined for all isotopes of interest from a known standard, and these factors are applied to the measured intensity ratios for conversion to concentration ratios.

The two primary contributors to the instrumental sensitivity factors of an ICP mass spectrometer are the first ionization potential of the ion and mass discrimination. Mass discrimination occurs at the skimmer cone, where ions first enter the mass spectrometer. There light ions are preferentially scattered out of the flight path relative to heavy ions, by space-charge effects. To a first-order approximation, this discrimination is proportional to the atomic mass. High-FIP atoms are less likely to be ionized in the plasma torch and will therefore be detected at lower intensities than low-FIP atoms. Within the range of elements considered in this study, the FIP contribution to instrumental sensitivity is tens of percent, but a highly nonlinear effect would be observed for elements with FIP > 10 eV.

All of the concentrations in the meteorites studied here were calculated via intensity ratios to Co, which has been independently determined for each sample. Mean measurements of Co (7590 ppm) and Ir (23.2 ppm)[15] from the Hoba meteorite were used to estimate instrumental corrections for all other measurements; relative sensitivity factors (RSF) for the elements were assumed to be a linear function of mass. In this method of calibration, the effect, for example, of FIP on instrumental sensitivity has been ignored. A more accurate means of calibration would employ relative sensitivity factors determined independently for each element of interest from a standard of known composition. The calibration used here was considered sufficient for the present discussion.

Point Analysis Mode. In this method of data collection, the laser is trained on one spot and a single pulse or brief train of pulses is used to ablate a small hole on the sample surface. This mode allows maximum spatial resolution to be achieved while compromising sensitivity and precision due to low sampling volumes. The signal pulse detected by the mass spectrometer is characterized by a steep rise to a peak followed by an exponential washout. Because of the unsteady count rates inherent in point analyses, rapid magnet scans are usually employed to avoid significant errors in measured ion ratios; however, this decreases the instrument's time on peak, further compromising the utilization of the signal and the precision. If a large number of masses is to be measured over a wide range (>20%), then one can either introduce a spray chamber to slow the signal variation or apply a drift correction for the measured signal pulse shape. Point analysis is best suited for measuring only a few ranges of masses. In the measurements below, for example, three mass ranges comprising nine elements are examined using point analyses.

Line Scan Mode. A line scan is generated by moving the sample under the pulsing laser beam using the software-controlled, motorized stage. Software supplied with the LSX-200 allows the scan rate and the line program (e.g., straight, repeat itself, or zigzag across a rectangular area with controllable spacing between passes) to be user-controlled. This method of analysis allows high, steady count rates to be attained by ablating a larger sample volume than that usually available for point analysis. The signal output from the line scan can be integrated into one measurement or analyzed as a continuous series of point analyses, with heterogeneities in the sample appearing as variations in the signal over time. In the latter case, it is important that the scan rate be slow compared to the signal washout time and the compositional changes in the sample. Chemical zoning can be resolved at spatial scales of 10−20 μm. An example of this use of the line scan is given below in the analysis of PGE distribution across taenite lamellae in iron meteorites.

Because of the high sample removal rates that are possible in line scan analyses, the ejecta and condensation blankets that form around the laser-ablated path can become noticeable. As an example, the area surrounding a laser path on the meteorite Hoba is depicted in an SEM image in Figure 3. Note that the particle size and particle density both diminish with distance from the laser path. The relative proportions of this material contributed by melt ejection and by condensation from the laser-produced

(14) Kaiser, T.; Wasserburg, G. J. *Geochim. Cosmochim. Acta* **1983**, *47*, 43.

(15) Rasmussen, K. L.; Malvin, D. J.; Buchwald, V. F.; Wasson, J. T. *Geochim. Cosmochim. Acta* **1984**, *48*, 805.

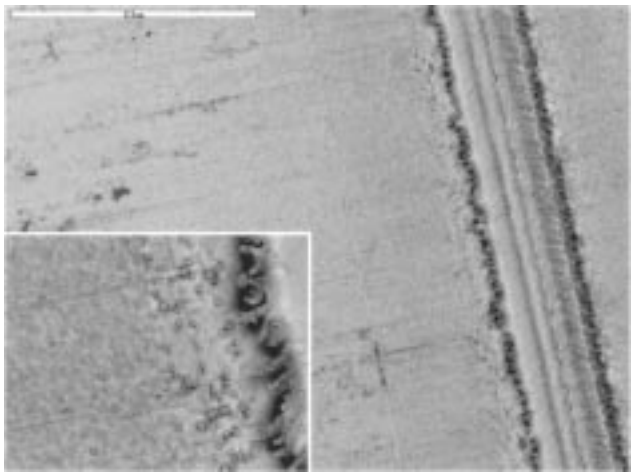

Figure 3. SEM image of the region surrounding a laser-ablated line scan on the iron meteorite, Hoba. Laser-ablated material has condensed from the laser-produced plasma onto the sample surface. Closer to the line scan, large melt blobs have been ejected from the ablated region. Scale bar, 500 μm. Inset is magnified by 3×.

plasma are unknown.

Depth Profiling. By repeatedly ablating material from the same point or area of the sample surface, laser ablation microanalysis allows compositional information to be acquired as a function of depth in the sample. Depth profiling of this sort can be performed at a single spot or by repeating line scans over the same path on the sample surface. An advantage of this technique is that the mean sampling depth can be as small as 0.1 μm, providing fine spatial resolution in the *z*-direction (normal to the sample surface). However, the same rules of signal strength scaling with sampling volume apply, so very low concentration analyses may require greater sampling depths. In addition, the laser beam profile is not a step function, so wall effects may have to be considered in some cases, particularly when the depth becomes large compared to the area being probed. Nevertheless, laser ablation depth profiling promises to provide compositional analyses on an even finer resolution than the lateral width of the laser beam. An example of depth profiling is given below in the analysis of surface impurities on iron meteorites.

Chemical Fractionation during Ablation. It was common in previous laser microprobe analyses[10,12,16] to take measurements over a long duration while drilling a hole at a single point. These authors observed serious chemical fractionation effects that presented themselves as time-dependent signals and varying element ratios in particular. As shown in Figure 4, this fractionation is avoided by performing a line scan over the surface of the sample rather than drilling into it. A pair of experiments is presented in Figure 4: in one, a line scan is shown of Pb and Th in a NIST 612 standard silicate glass; in the other experiment, the same analysis was carried out while the laser drilled a hole into the sample. It is evident that both the elemental ratios and the absolute intensities displayed much less variation during the line scan than while hole drilling. Much of the chemical fractionation discussed in previous studies (e.g., ref 10) may have arisen from geometrical effects while drilling too deeply into the sample. The line scan capabilities of the LSX-200 thus allow more reliable interelement ratios to be measured.

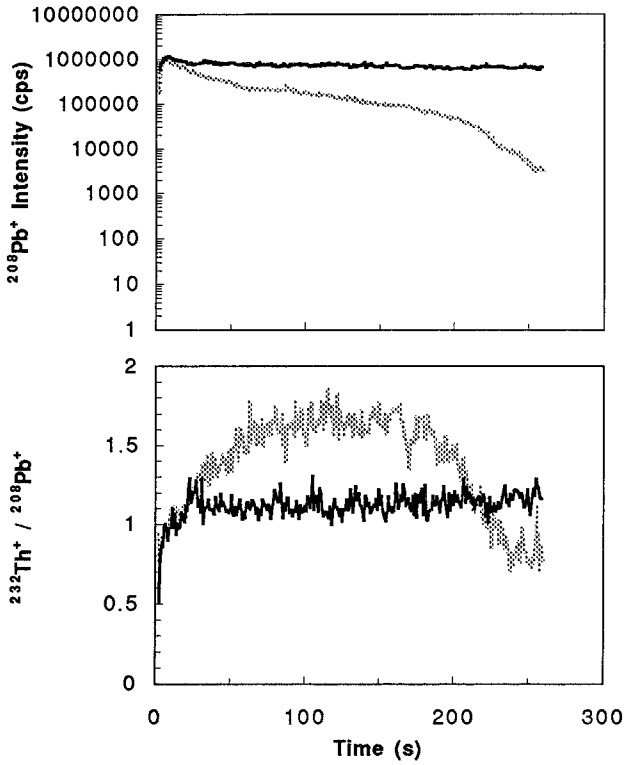

Figure 4. Pb and Th in a NIST 612 silicate glass standard. The heavy line represents a line scan measurement, and the light line represents a hole-drilling measurement. The signal intensities and the interelement ratios exhibit much more variation while hole drilling than during a line scan.

RESULTS AND DISCUSSION

Bulk Composition of Iron Meteorites. To illustrate the relative advantages of point analyses and line analyses, the PGE composition of the group IVB iron meteorite Hoba was measured using these two laser ablation methods. Hoba was selected because the IVB irons are highly homogeneous on a fine scale; therefore, the two analyses should be expected to yield the same results regardless of the difference in spatial resolution. Typical operating conditions for the laser microprobe are listed in Table 1. Five point analyses, from a laser-ablated spot ~35 μm in diameter, were performed using a 10-Hz train of 60 laser pulses, each having an energy of 0.2 mJ. Five line analyses were performed using lines 4.5 mm in length, scanned at a rate of 50 μm/s with the laser operating at 1.5 mJ and 10 Hz.

Results are summarized in Table 2, which lists the mean and standard deviation (1σ) of five analyses for each element. No error is given for Co because this element was used to normalize the other results. As expected, much higher precisions are achieved by sacrificing spatial resolution and using a line scan. Standard deviations of the measurements were typically reduced by a factor of about 20, to ~2%, when much larger sample volumes were analyzed. Discrepancies with the quoted literature values can be attributed to inadequacies in the calibration method, discussed above, and perhaps to large-scale heterogeneities between the natural samples. (Further tests in our laboratory have suggested that the Au measurements in particular require better standardization.) Detection limits are given as 3σ of the background, based

(16) Hirata, T.; Nesbitt, R. W. *Geochim. Cosmochim. Acta* **1995**, *59*, 2491.

Table 1. Laser Microprobe Operating Conditions

mass spectrometer	
detector mode	analog (Co); counting (PGEs)
sweep mode	peak hopping
settle time	1 ms/amu
dwell time	0.020 s
no. of sweeps	60
resolution	340
ICP ion source	
frequency	27.12 MHz
power	1345 W forward; <6 W backward
Ar flow rates	
cooling	14.1 L/min
auxiliary	1.1 L/min
carrier	1.6 L/min
laser ablation	
beam	266 nm
diameter	20−40 μm
pulse energy	0.2 mJ
pulse repetition	10 Hz
no. of pulses (point analysis)	60
scan rate (line scan analysis)	5 μm/s

Table 2. Hoba PGE Analyses

	point analyses			line scan analyses			lit.
	ppm	std dev	det limit	ppm	std dev	det limit	values[a] (ppm)
Co	≡7590.0			≡7590.00			7590.00
Ru	32.2	12.7	1.39	35.31	0.26	0.0139	30.93
Rh	3.3	0.5	2.96	3.59	0.05	0.0016	4.94
Pd	7.8	5.5	9.31	6.10	0.09	0.0072	7.00
Re	2.9	1.3	0.65	3.71	0.07	0.0015	2.85
Os	34.0	11.9	2.02	43.27	0.97	0.0004	40.96
Ir	≡23.2	8.9	0.36	≡23.20	0.49	0.0002	23.20
Pt	17.8	7.0	0.22	15.63	0.25	0.0008	28.78
Au	0.06	0.19	0.07	0.0245	0.0010	0.0003	0.08

[a] Literature values are taken from ref 15 (Co, Ir, Au), ref 23 (Ru, Pt), ref 24 (Rh), ref 14 (Pd), and ref 8 (Re, Os). Co and Ir values are fixed as part of the calibration (see text).

on three measurements of the background intensity with the laser turned off. These limits are strong functions of the count rate and may vary greatly when experimental conditions are changed. Although the point analyses are admittedly permissive, it is nevertheless important to note that the two analyses gave consistent data within the errors. The line scan results presented in Table 2 reflect optimal conditions, where the sample was homogeneous over a length scale of millimeters. A more typical application in meteoritic studies might involve a shorter line scan; for example, an analysis of 250 μm line scans on kamacite in Grant produced standard deviations of 5−9% for ppm-level concentrations of PGEs.

Similar analyses of PGEs in several irons (Hoba IVB, Negrillos IIA, kamacite in Grant IIIB, kamacite in the pallasite Imilac) are shown in Figure 5. These data were all obtained from an average of five point analyses, with a beam diameter of 20−40 μm, yielding a crater of approximately 3−5 μm depth (crater volume ~1−6 pL). The calibration described above for the Hoba meteorite was used for all meteorites indicated in Figure 5. Missing data indicate that the element was either not analyzed for or that the measured concentration was within one standard error of the background intensity. Comparison with literature values indicates good agreement in the shape of the pattern, and even in the absolute values.

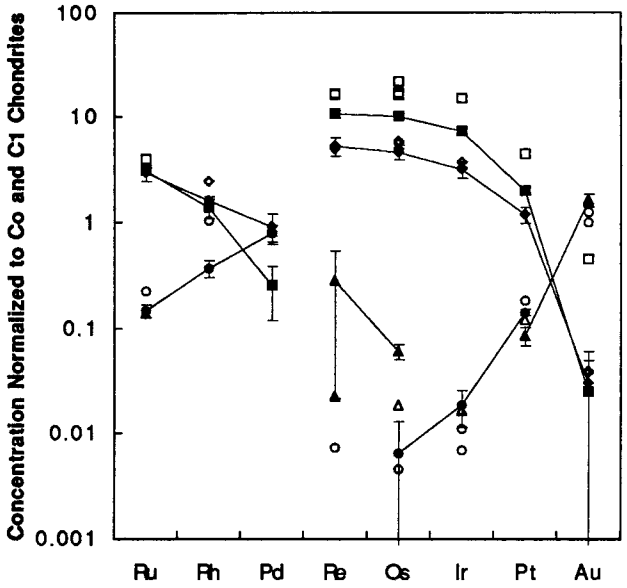

Figure 5. Analyses of PGEs by laser ablation ICPMS (filled symbols) in three iron meteorites and the iron of one pallasite. Literature data (open symbols) for bulk metal are shown. Data sources: Hoba (diamonds: refs 8, 14, 15, 24, 25), Negrillos (squares: refs 8, 26, 27), Grant kamacite (circles: refs 24, 26), and Imilac kamacite (triangles: refs 5, 28). Calibration procedures are described in the text.

The precision of analyses for most measurements is limited by signal stability, although counting statistics become important at low concentrations. As demonstrated in Table 2, the precision of all measurements could be significantly improved by increasing the crater volume, thereby sacrificing spatial resolution.

Surface Contamination of Hoba Specimen. A sequence of line scans, each performed over the same path on the surface of Hoba, revealed that some elements were concentrated on the surface of the specimen studied; it is likely that this contamination is the product of sample preparation such as sawing the specimen from a larger piece and subsequent polishing. The concentration of several elements is plotted as a function of depth from the surface in Figure 6. The depth values in this figure are estimated from separately determined ablation rate experiments. As shown in Figure 6, contaminants such as Cu and W decrease as the surface is gradually removed by laser ablation, while the concentration of other elements holds steady (±1−3%) with depth.

There are many applications of depth profiling to the study of meteorites. Since the beam diameter is ~20 μm, searching for elemental enrichments occurring at grain contacts is best done by depth profiling, which is expected to have finer resolution. Such enrichments may be expected where oxidation of the metal has taken place, e.g., at olivine−metal contacts in pallasites, or where sulfidation of metal has taken place, e.g., at sulfide−metal contacts around sulfide-rimmed metal grains in chondrules.[17]

M-Distribution of PGEs in Taenite Lamella. Figure 7 shows Ru, Rh, and Pd distributions, exhibiting the characteristic M-shape, across a single taenite lamella in the Grant meteorite (group IIIB). These profiles were measured by scanning the laser slowly (at 5 μm/s) across the meteorite surface while rapidly sweeping the

(17) Rambaldi, E. R.; Wasson, J. T. *Geochim. Cosmochim. Acta* **1981**, *45*, 1001. Zanda, B.; Bourotdenise, M.; Hewins, R. H. *Meteoritics* **1995**, *30*, 605.

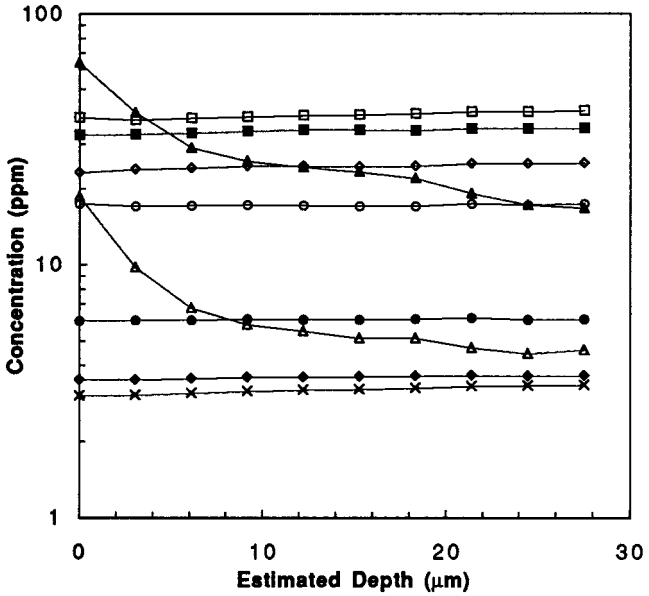

Figure 6. Concentrations of various elements in the iron meteorite Hoba as a function of depth in the specimen. These depth profiles were acquired by repeatedly scanning the laser over the same path on the meteorite. The depth values have been approximated using the estimated ablation rates in this sample. Key: (open up-triangle) Cu, (filled square) Ru, (filled diamond) Rh, (filled circle) Pd, (filled up-triangle) W, (open down-triangle) Re, (open square) Os, (open diamond) Ir, and (open circle) Pt.

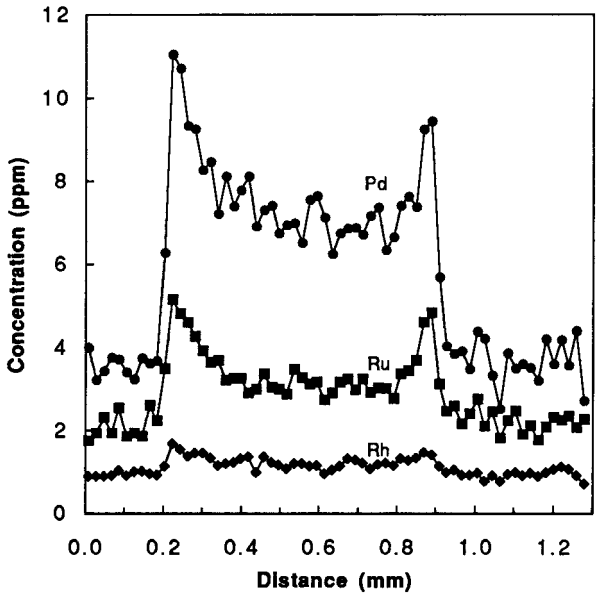

Figure 7. Concentration profiles of Ru (square), Rh (diamond), and Pd (circle) across a taenite lamella in the Grant IIIB iron. The flat regions on both sides are measurements from the kamacite phase. The characteristic M-shape is the result of partitioning between the two phases and slow diffusion in the taenite phase.

mass spectrum to measure Fe, Co, Ni, Ru, Rh, and Pd. The Fe, Co, and Ni intensities were used to internally standardize the LPGE concentrations. The laser beam path was 40 μm wide, and each point in Figure 7 represents the signal collected over 20 μm of travel by the laser. The signal washout ($\sim$ order of magnitude/5 s) is short compared to the scan rate, as evident in the sharpness of intensity dropoff on the right-hand side of the figure.

Comparison with Other Techniques. *(i) Ion Microprobe.* Recently Hsu et al.[1] reported an ion microprobe method for analysis of Os, Ir, Pt, and Au using negative ions on $\sim$20 μm spots in iron meteorites, followed by further reports of the application of this method to chondritic metals.[18] Ion yields for Ru, Rh, Pd, and Re were below detection limits for this technique.[1] Furthermore, Hsu et al.[1] found that "[i]on yields for Fe, Ni, and Co covary by up to a factor of 5 over the course of a measurement" and were not reproducible from spot to spot; therefore they monitored their primary Cs^+ ion beam intensity to normalize the secondary ion signals for the PGEs. With laser ablation microanalysis, the sensitivity is higher by 1−2 orders of magnitude for the same volume of material ablated, and the ion yield (positively correlated with mass) is only a factor of $\sim$2 lower for the light PGEs (Ru−Pd) relative to the heavy PGEs (Os−Au), with stable intensities ($\pm$1−10%). The spatial resolution shown in Figure 7 is also much finer than that demonstrated by Hsu et al.[1] (one point per 80 μm) using an ion microprobe to measure M-distributions of PGEs.

(ii) Laser Ablation-Quadrupole ICPMS. Hirata and Nesbitt[11] reported PGEs and Re on iron meteorites using a Nd:YAG UV (266-nm) laser ablation system attached to a quadrupole ICPMS (VG PQ3 with S-option). Their measurements can be compared directly to those of the present study. They reported a smaller spot size (12−15 μm), but their spots are deeper (30 μm), resulting in similar sampling volumes (3−5 vs 2−6 pL). The spatial resolution indicated in the figures of Hirata and Nesbitt[11] is much coarser (50−125 μm) than their reported spot size. Because of the absence of white noise in the Element, systematically lower backgrounds are attained, and better precision is also achieved, using the methods described in the present report. The conclusions of Hirata and Nesbitt[11] that the PGEs (with the exception of Pd) do not partition preferentially into taenite during kamacite exsolution in iron meteorites, are diametrically opposed to those of Rasmussen et al.,[19] Hsu et al.,[1] and the present study. No explanation for this discrepancy is apparent.

(iii) Laser Ablation Multicollector ICPMS. Christensen et al.[20] used laser ablation with a multicollector ICPMS to determine Pb isotopes with high precision in Fe−Mn crusts. PGE analyses appear not to have been performed yet with this system. Multicollection is an ideal means of overcoming the transient nature of laser ablation signals,[21] but present high-resolution instruments[20,22] are restricted to Faraday cup collector assemblies that

(18) Hsu, W.; Huss, G. R.; Wasserburg, G. J. *Lunar Planet. Sci. Conf.* **1998**, *29*, 1939. Connolly, H. C., Jr.; Huss, G. R.; Hsu, W.; Wasserburg, G. J. *Lunar Planet. Sci. Conf.* **1998**, *29*, 1893.
(19) Rasmussen, K. L.; Malvin, D. J.; Wasson, J. T. *Meteoritics* **1988**, *23*, 107.
(20) Christensen, J. H.; Halliday, A. N.; Godfrey, L. V.; Hein, J. R.; Rea, D. K. *Science* **1997**, *277*, 913.
(21) Cromwell, E. F.; Arrowsmith, P. *J. Am. Soc. Mass Spectrom.* **1996**, *7*, 458.
(22) Hirata, T.; Hattori, M.; Tanaka, T. *Chem. Geol.* **1998**, *144*, 269.
(23) Humayun, M.; Campbell, A. J. Unpublished work, University of Chicago, 1998.
(24) Ryan, D. E., Holzbecher, J.; Brooks, R. R. *Chem. Geol.* **1990**, *85*, 295.
(25) Hirata, T.; Masuda, A. *Meteoritics* **1992**, *27*, 568.
(26) Buchwald, V. F. *Handbook of Iron Meteorites*, University of California Press: Berkeley, 1975. Pernicka, E.; Wasson, J. T. *Geochim. Cosmochim. Acta* **1987**, *51*, 1717.
(27) Morgan, J. W.; Horan, M. F.; Walker, R. J.; Grossman, J. N. *Geochim. Cosmochim. Acta* **1995**, *59*, 2331. Blum, J. D.; Pellin, M. J.; Calaway, W. F.; Young, C. E.; Gruen, D. M.; Hutcheon, I. D.; Wasserburg, G. J. *Geochim. Cosmochim. Acta* **1990**, *54*, 875.
(28) Scott, E. R. D. *Geochim. Cosmochim. Acta* **1977**, *41*, 349.

require very high signals; the crater volume of Christensen et al.[20] was 1000 times larger than that reported here. The signals analyzed in the present work, using a secondary electron multiplier operating in ion counting, are well below the detection limits of a Faraday cup detector system. Hirata et al.[22] determined Os isotopes and elemental signals of $^{183}W/^{188}Os$ using a multicollector ICPMS, applying laser ablation as a solid sampling tool on naturally occurring iridosmine (Ir, Os) alloys. Application of the multicollector ICPMS required >1000 ppm Os, a concentration 10^3-10^9 times higher than found in naturally occurring materials, except a few ores.

In summary, the laser ablation system provides an accurate means of solid sampling for magnetic sector ICPMS, allowing both the determination of bulk metal composition and chemical zoning within the sample at a spatial resolution of ~20 μm and a sensitivity in the ppb−ppm range for metal matrixes. This technique is comparable to or better than other techniques and can be directly applied to trace elements in metallic matrixes including metal grains occurring in chondritic meteorites, metals from archeological artifacts, and industrial metals. The methods can also be generally applied to the determination of trace elements in other matrixes including silicates, oxides, and sulfides, after establishing experimental parameters appropriate to the ablation characteristics of these specific matrixes.

ACKNOWLEDGMENT

Meteorite specimens were generously donated by the National Museum of Natural History (Smithsonian Institution), courtesy of Linda Schramm and Glenn J. MacPherson. Personnel at CETAC Technologies, Inc., including Donn Vanden Bosch, Ted Howe, and Tony Vaccaro, are thanked for their assistance in setting up the laser ablation apparatus. The assistance of Andy Davis with the SEM is gratefully acknowledged. Discussions with numerous colleagues, including Steve Shuttleworth, Mike Schmidt, and Jim Zhu, have been invaluable. The manuscript was improved by comments from Andy Davis, Steve Simon, and the reviewers. The instrumentation for this research was funded by NSF Grant EAR-9601478 and by The University of Chicago. A.J.C. acknowledges support from DOE Grant DOE DE-FG02-97ER14773 (to F. M. Richter).

Received for review July 29, 1998. Accepted December 9, 1998.

AC9808425